



Parametric study and optimization of pillow-plate heat exchanger using multi-objective genetic algorithm and entropy generation minimization approaches

Mohsen Tavallaei¹ · Mahmood Farzaneh-Gord² · Ali Jabari Moghadam¹ · Amir Ebrahimi-Moghadam³

Received: 8 April 2022 / Accepted: 29 March 2023 / Published online: 15 April 2023
© The Author(s), under exclusive licence to Springer-Verlag GmbH Germany, part of Springer Nature 2023

Abstract

The pillow-plate heat exchanger (PPHE) is a kind of heat exchanger constructed by a set of wavy surfaces like a pillow. In this study, the influence of pillow-plate geometrical parameters (including dimensionless channel height, dimensionless plate width, and pillow plates number) and flow specification (including Reynolds and Prandtl numbers) in terms of derived dimensionless parameters on their thermo-hydraulic performance is evaluated through a comprehensive parametric investigation. The fully developed regime in PPHE channel is assumed and fluid flow, heat transfer, and thermodynamics principles are combined in terms of the entropy generation minimization (EGM) approach. Afterwards, a multi-objective optimization method is applied by using the non-dominated sorting genetic algorithm (NSGA-II) to find the optimal design of PPHE. In this way, the maximization of performance evaluation criterion (PEC) against the minimum total entropy generation for PPHE is eventuated. The behavior of PPHE's important evaluation criteria are illustrated for different Reynolds numbers from 1000 to 6000 by varying Prandtl number and the proposed dimensionless geometry parameters. Also, contrariness between two parts of non-dimensional entropy generation (NDEG), i.e., thermal and frictional, is concluded from the result for Pareto-optimal front. It indicates there is an optimum Re number that minimizes $(NDEG)_{tot}$ at any geometrical parameters. On the other hand, multi-objective optimization results show the conflict between two main objective functions namely PEC and $(NDEG)_{tot}$ that reveals any geometrical change to increase in the PEC of heat exchanger leads rising in total entropy generation and vice versa. The final optimum values of the objective functions are $PEC_{opt} = 1.3712$ and $(NDEG)_{tot,opt} = 0.0145$ which occurs at $Re = 3265$.

Nomenclature

A Heat transfer area, m^2
 C_p Specific heat capacity of the fluid, $J/(kg.K)$

d Diameter, m
 e_i Inner channel height, m
 e Outer channel height, m
 f Friction factor, -
 G Mass flux, $kg/(m^2.s)$
 h Heat transfer coefficient, $W/(m^2.K)$
 k Thermal conductivity, $W/(m.K)$
 L Height of the pillow plate, m
 \dot{m} Mass flow rate, kg/s
 N Number of plates row, -
 Nu Nusselt number, -
PEC Performance evaluation criteria, -
Pr Prandtl number, -
NDEG Non-dimensional Entropy generation, -
 t_w Wall thickness, m
Re Reynolds number, -
 R_f Thermal resistance of fouling, $(m^2.K)/W$
 S_T Transversal distance between welding spots, m
 S_{gen} Entropy generation, $W/(m.K)$
 S_L Longitudinal distance between welding spots, m

✉ Mahmood Farzaneh-Gord
m.farzanehgord@um.ac.ir
Mohsen Tavallaei
tavallaeimohsen@shahroodut.ac.ir
Ali Jabari Moghadam
alijabari@shahroodut.ac.ir
Amir Ebrahimi-Moghadam
amir_ebrahimi_051@yahoo.com

¹ Faculty of Mechanical Engineering, Shahrood University of Technology, Shahrood, Iran
² Mechanical Engineering Department, Faculty of Engineering, Ferdowsi University of Mashhad, Mashhad, Iran
³ Mechanical Engineering Department, Faculty of Engineering, Quchan University of Technology, Quchan, Iran

ΔP	Pressure drop, kPa
ΔT	Temperature difference, K
U	Overall heat transfer coefficient, $W/(m^2 \cdot K)$
V	Channel flow velocity, m/s
w	Dimensionless plate width, -
W_e	Width of edges of the pillow plate, m
Q	Heat load, kW

Subscripts

hyd	Hydraulic
sp	Spot welding point
p	Pillow plate
ΔT	Thermal
ΔP	Frictional
tot	Total

Greek symbols

μ	Fluid dynamic viscosity, Pa-s
ρ	Density, kg/m^3
η	Efficiency

1 Introduction

Heat exchangers (HEs), as devices that are utilized for exchanging heat and thermal energy between fluids, are considered a noticeable component in different industrial applications such as power generation. These devices have been employed to exchange heat among two or more fluids or between a fluid and a rigid plane at different temperatures and in thermal contact. Various HEs have been used in many thermal engineering and energy systems [1–5]. Plate HE (PHE) is a kind of HEs that includes some thin plains or wavy plates separating hot and cold fluids. PHE offers a lot of advantages that make it many attractive HE in industrial applications. From these advantages, it could be named to their expandability, high efficiency, easy cleaning and removing, and lower related costs compared to the other kinds of HEs [6, 7]. The distinguishing features of PHEs are their high surface area density and thermal effectiveness, resulting in reduced size, weight, and space compared to other types of HEs [8]. Nowadays, the growing attention to developing an efficient type of HE has urged researchers to improve the design of geometries and features of PHEs for different applications. So, a novel type of PFHE as the Pillow-Plate Heat Exchanger (PPHE) has been investigated towards the better geometry of plates and welded construction with the different cross-sectional areas of fluid channels, low cost of production, and small pressure drop of HEs. The PPHEs have wide practical uses in different industries. This type of HE was initially proposed to be applied in the

food industry [9] and because of their advantages, they were later used in other industries such as chemical and oil refining industry [10], thermal energy production/storage systems [11], refrigerating application [12] and etc.

PPHE consists of two metallic sheets which are point-welded over the whole surface according to a specific pattern, whereas the edges are continuously seam welded. The inner channel of PPHE has a complex shape that locates between the sheets by applying the hydroforming technique. The PPHE construction could be considered as multiple panels of pillow-plate located together adjacently. This arrangement of panels configures the outer and inner channels alternatively as heat exchanging zones. So, there are two channels for heat transferring which one is built between two neighbor panels of welded pillow-plate as an outer channel and another is formed inside a panel of welded pillow-plate as an inner channel. This leads to considering hydraulic diameters and cross-sectional areas for channels. It should be noted that the technology for manufacturing PPHEs is commutable and their geometries are involved in a wide diversity [13]. The main feature of PPHE is the wavy surfaces in the shape of a pillow that improves heat transfer between fluids. In other words, the special geometry of this kind of HE affects thermal performance. High operating pressure, sealed construction, and pretty light weight are other features of the PPHE in comparison of other HEs [14].

In the available literature, some studies had focused on the evaluation of the heat transfer and flow characteristics in PPHEs based on numerical and experimental works. Dormohammadi et al. [15] investigated the entropy generation minimization (EGM) approach for heat transfer optimization through a wavy channel by using nanofluid. They discretized equations by employing finite volume method. Results of their work showed that the Nusselt number (Nu) increases by an increase in volume fraction of nanoparticles. Arsenyeva et al. [16] concentrated on the design of PPHE by considering the minimum heat transfer area. They tried to find pressure drop and heat transfer coefficient inside the HE by assuming the single-phase working fluid. Piper et al. [17] directed simulations by CFD (Computational Fluid Dynamics) method for a particular geometry of pillow-plate that flow streams of heat exchanging were in a turbulent manner. Their work resulted in the suggestion of correlations for the heat transfer and friction factor coefficients. In another work by the same research group, Piper et al. [18] carried out a detailed study of turbulent fluid flow within a pillow-plate panel based on CFD for several geometries. The simulations revealed that the pillow-plate channel coefficient of heat transfer was proportional to $Re^{0.79}$ and $Pr^{0.38}$. The conclusion of their work stated that increasing the Re number

causes decreasing in the thermo-hydraulic efficiency of the pillow plate channel that highest efficiency is achieved at the $Re = 1000$. In another investigation, the experimental evaluation of heat transfer and coefficient pressure drop for inner channels of PPHE for a single-phase fluid flow by considering different geometries was presented by Tran et al. [19]. They proposed the relations for heat transfer coefficient and friction factor depending on the geometry of the pillow-plate panel. In other research, Tran et al. [20] carried out single-phase fluid flow and two-phase condensation heat transfer experiments on different pillow plate geometries as numerical results were compared with results obtained with the bundle of plain and rough tubes. Measurements expressed the total relative uncertainties below 3% for the coefficients of heat transfer in cooling-side and below 2% for pressure drop. Also, the derived correlations for Nu number and friction coefficient are validated for $300 < Re < 10,000$ and $2 < Pr < 80$. Mitrovic and Peterson [21] experimentally studied forced convection heat transfer in the PPHE with oil and distilled water as the working fluids. Piper et al. [22] tried to simulate the hydroforming process by using Finite Element Analysis (FEA) to obtain the wavy profile to reach realistic profiles. The simulation results illustrated that the surface area enlargement from the waviness is about 2–7% in relation to a plane surface. Mitrovic and Maletic [23] carried out varying geometrical and process parameters for the pillow plate channel by numerical simulations. They considered heat transfer of single-phase fluid flow inside the channel as an objective to be maximized. The presented results showed that for Re numbers greater than 500, the PPHE Nu number was higher than the flat channel; and for Re numbers less than 500, the secondary flows became weak and heat transfer caused by the recirculation zones and Nu is fallen, consequently. Geometrical optimization for panels of pillow-plate was taken into account by several approaches, such as asymmetrical changes in the diameter of round welding points or variation in the welding spots patterns like distances between these spots [24]. Alizadeh and Ganji [25] investigated the effects of using longitudinal fins on the outside of the two-phase thermosyphon condenser by developing the central composite design approach. They considered thermal resistance and efficiency of thermosyphon as the system responses and employed an optimization procedure by response surface methodology. Optimization results showed that $0.168^{\circ}C/W$ as a lowest thermal resistance and 93.89% as a highest efficiency. In another study, Alizadeh et al. [26] developed a numerical model and they optimized producer of the solidification process by using nanoparticles within a latent heat thermal storage system. They employed response surface method for fin geometry optimization and considered solidification time as the objective function. Optimization result illustrated 1269 s for completing the

solidification by given fin configuration which leads to a reduction of 61.54% in solidification time.

As another category in the field of study, one of the practical tools for assessing the heat transfer improvement is the analysis based on the second law of thermodynamics by consideration of both trade-off factors. The EGM method as a thermodynamic-based optimization is employed as a criterion for optimal analysis to evaluate the thermal performance of any system. The EGM is working based on the identification and formulation of irreversibilities due to heat and mass transfer or simply fluid flow [27]. The performance assessment criteria for HEs are generally distinguished into two groups based on the first law of thermodynamics and based on the combination of the first and second laws of thermodynamics. Recently, the second group has been more attractive and noticeable. Often, the heat transfer in HEs involves the heat transfer under limited temperature difference and the fluid friction under finite pressure drop that these thermodynamic processes are identified as irreversible non-equilibrium processes [28]. Maximum efficiency and minimum exergy loss together with minimum heat transfer area for a particular application are two important issues in the design of HEs. So, optimization of HEs is necessary to reach the best of these objectives.

Hence, a good criterion for geometric optimization performance evaluation of various types of HEs is EGM which is widely applicable. Bejan [29] investigated the relationship between dimensionless entropy generation and heat transfer effectiveness in cases of frictionless fluid flow. Recently researchers paid attention to carrying out studies about the optimization of HEs. Zhou et al. [30] studied the second law of thermodynamics for thermal systems and reached the parameters for the optimal design of a plate-fin HE corresponding to this law. Farzaneh-Gord et al. [31] carried out an optimization of concentric tubes helical HE analytically in the view of thermodynamic. Results of their work presented optimal geometrical parameter values for flow streams in turbulent and laminar conditions. Sodagar-Abardeh et al. [32] investigated chevron plate heat exchanger geometry optimization using the EGM method. They studied the effects of geometrical parameters as results showed that there are the optimum values for each of them. Also, they found that each variable could minimize the entropy generation. For example, the minimum value of entropy generation occurred at surface enlargement parameter and chevron angle of 1.27 and 46° , respectively. A combination of the EGM and genetic algorithm methods was used by Guo et al. [33] and several geometrical parameters of the shell and tube HE were optimized by them. Their work aimed to minimize dimensionless entropy generation by considering a finite temperature difference and pressure drop. Results indicated that the Pareto optimal solutions were trade-off between the

pumping power and heat exchanger effectiveness that the required pumping power was 260 W for the effectiveness of about 0.71. Shi and Dong [34] studied the entropy generation of a rotating helical tube HE to optimize total entropy generation and parts of it. Investigation of heat transfer and entropy generation of three various types of HEs carried out by et al. [35] that they evaluated the usability of nanofluid as a coolant for a HE. A combination of the EGM approach and genetic algorithm was used by Ebrahimi-Moghadam and Moghadam [36] to optimization of geometric and hydrodynamic parameters for the corrugated HEs. They employed Al_2O_3 nanoparticles in water and their results illustrated that adding nanoparticles promoted heat transfer. However, there was a little increment in irreversibility which 5% rising in irreversibility caused by adding 4% nanoparticles. Deymi-Dashtebayaz et al. [37] prepared a parametric thermo-hydraulic study based on the optimization of CuO/water nanofluid flow inside dimpled heat exchangers through the combination of the mass and heat transfer and the second law of thermodynamics. Results showed that the effects of the flow mean temperature and HE pitch ratio on the entropy generation were the lowest and highest, respectively. Also, the optimization producer revealed that optimum Re number, pitch ratio, non-dimensional flow mean temperature, and fraction factor were 4610, 0.00326, 1.077, and 0.000216, respectively. Rostami et al. [38] studied the solidification process of a phase change material (PCM) in a maple leaf-shaped storage system. They carried out numerical investigation to enhance the heat transfer using nanoparticles as the direct and indirect methods. Optimization was done to accelerate the solidification process and decrease its time. Optimized results show that the leaf form veins fins reduce solidification time as 42.6% which is much more effective than making nano-enhanced phase change material with a 25.5% time reduction. Alizadeh et al. [39] investigated the role of new branching fins and nanoparticles to increase the heat transfer and their effects on the solidification of a PCM within a hexagonal storage. They studied the phase-change process during the time-dependent boundary conditions together with exergy efficiency of the system. Also, they used the finite element method to simulate the procedure. Results indicated the employing innovative fin was more effective than making nano-enhanced phase change material by 30% solidification time reduction. Kotcioglu et al. [40] considered a cross-flow HE and made an entropy generation minimization based on the second law analysis of it. Yousefi et al. [41] implemented a PFHE optimization by minimizing the number of total entropy generation units under a certain pressure drop and heat load by applying the competitive algorithm. Alizadeh and Ganji [42] conducted the experimental study on thermal performance of an externally finned thermosyphon. They developed empirical correlations to obtain evaporator and condenser heat transfer coefficients.

Response surface method was applied to optimize the thermosyphon operating parameters to achieve the best performance. Results showed that the presented correlations have a high accuracy to predict mentioned coefficients.

Taking into account the available published studies, there are many kinds of research, investigated the heat transfer and flow characteristics of the PPHEs based on different numerical and experimental approaches. It could be realized, despite studies around the second-law-based optimization of the HEs, there is not any investigation about the optimization of the PPHEs based on the second law of thermodynamics. Accordingly, to fulfill this gap, a parametric model based on the EGM method is firstly developed for evaluating the sensitivity of the thermo-hydraulic criteria of the PPHE to the design parameters, including both geometrical and flow parameters. This method could be considered as a bridge between heat transfer and fluid mechanics (a robust objective for the assessment of PPHEs). To make the study even more comprehensive, the performance evaluation criterion (PEC) is also investigated as another function. Finally, the most appropriate design parameters and operating conditions are sought through a powerful multi-objective optimization procedure. The non-dominated sorting genetic algorithm (NSGA-II) is employed for multi-objective optimization of a PPHE while the entropy generation (to be minimized) and performance evaluation criteria (to be maximized) are considered as two objective functions.

2 Methodology

2.1 Thermo-hydraulic design of PPHE

Since PPHE has a pretty complex geometry, the determination of all the geometrical design parameters such as hydraulic diameter and effective areas (including cross-sectional and total heat transfer area) is not an easy procedure. As shown in Fig. 1, the geometry is defined by the following parameters: spots welding diameter (d_{sp}), the longitudinal pitch (S_L) and transverse pitch (S_T) of weld spots, metal sheet thickness (t_w), maximum height of pillow plates due to inflation that is adjusting by specific pressure in the hydro-forming process (e_i), and distance between pillow panels that constructs the outer channel (e). These heights represent important design parameters of pillow plates. All of these geometrical parameters are illustrated in Fig. 1.

So, in this section, the determination of design parameters and influential parameters for PPHE is presented. Equivalent diameter and channel cross-sectional area of the inner and outer channels can be calculated respectively according to Eqs. (1–4) [22].

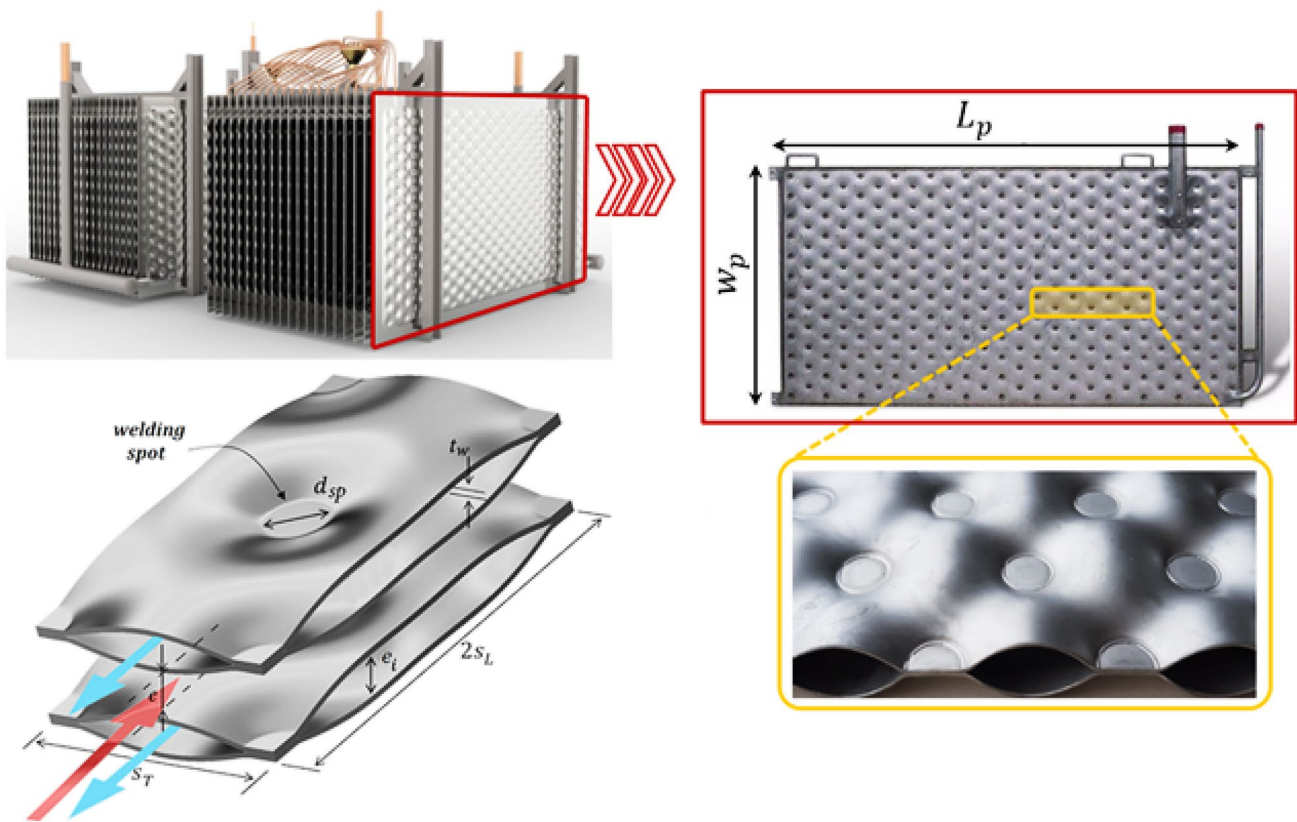


Fig. 1 The shape and geometrical parameter of pillow plate heat exchanger channel

$$d_{hyd,i} = (2/\sqrt{2})e_i \tag{1}$$

$$y_p = \frac{2S_L}{S_T} \tag{7}$$

$$d_{hyd,o} = (2/\sqrt{2}) \cdot [\sqrt{2}(e_i + e) - e_i] \tag{2}$$

$$A_{cs,i} = e_i \cdot (w_p - 2w_e) / \sqrt{2} \tag{3}$$

$$A_{cs,o} = [\sqrt{2}(e_i + e) - e_i] \cdot (w_p - 2w_e) / \sqrt{2} \tag{4}$$

In these relations, w_p is the plate width and w_e is the edge thickness of pillow plates.

In the current study, to present a better sense of role of pillow plate geometrical parameters on the results, the following dimensionless parameters can be used:

$$y_i = \frac{e_i}{S_T} \tag{5}$$

$$y_d = \frac{d_{sp}}{S_T} \tag{6}$$

Darcy friction factor, f , is described as a function of the Re number and is represented by a curve which can be approximated with a power-law function as following equation [16]:

$$f = n_1 Re^{m_1} \tag{8}$$

The adjustment parameters n_1 and m_1 in Eq. (8) were estimated by plotting f over the Re number carrying out in [18] by using CFD simulations. The Re number is expressed as Eq. (9) [43].

$$Re = \frac{G \cdot d_{hyd}}{\mu} = \frac{\dot{m} \cdot d_{hyd,i}}{\mu \cdot A_{cs}} \tag{9}$$

So, the pressure drop for channels can be defined as below:

$$\Delta P = f \frac{L_{ch} \cdot \rho \cdot V^2}{2d_{hyd}} \tag{10}$$

where, L_{ch} as an operative length of the pillow plate is described according to Eq. (11).

$$L_{ch} = L_p - 2w_e \quad (11)$$

For designing the PPHE in the sense of thermal consideration, the Dittus-Boelter type power-law function is used in this work that is based on dimensionless parameters. Accordingly, the power-law type equation for estimating the Nu number could be presented by Eq. (12) [16].

$$Nu = n_2 Re^{m_2} Pr^{m_3} \quad (12)$$

It should be noted that parameters n_2 , m_2 , and m_3 are dependent on the geometry of pillow-plate and are estimated numerically in [18] by the CFD approach.

The best-fit functions to estimate the parameters of n_1 , n_2 and m_1 , m_2 , m_3 in Eqs. (8) and (12) are expressed in Eqs. (13)–(17). The range of validation for the Re number is around 1000 to 8000 and for the Pr is 1 to 150 [18].

$$n_1 = 2.8y_i + 1.35y_d + 0.92 \quad (13)$$

$$n_2 = 0.711y_i - 0.163y_d + 0.022 \quad (14)$$

$$m_1 = 0.53y_i + 0.3y_d - 0.29 \quad (15)$$

$$m_2 = 0.29y_d - y_i + 0.8 \quad (16)$$

$$m_3 = 0.4 \quad (17)$$

As a result, by using Nu number relation, $Nu = h \cdot d_{hyd}/k$, the overall heat transfer coefficient is given by the inverse of convection heat transfer coefficients and thermal resistances presented in Eq. (18).

$$\frac{1}{U} = \frac{1}{h_i} + \frac{1}{h_o} + \frac{t_w}{k_w} + R_{f_i} + R_{f_o} \quad (18)$$

The total area of heat transfer for HE is calculated as follows [44, 45]:

$$A_{ht} = \frac{Q}{U \cdot \Delta T_{LMTD}} \quad (19)$$

$$\Delta T_{LMTD} = \frac{(T_{h,in} - T_{c,out}) - (T_{h,out} - T_{c,in})}{\ln\left(\frac{T_{h,in} - T_{c,out}}{T_{h,out} - T_{c,in}}\right)} \quad (20)$$

where, the values of ΔT_{LMTD} and heat duty (Q) are specified by the steams conditions are known. All other parameters depend on the design of HE and geometry of its channel such as the number, size, and geometry of plates that changing them can cause different channel geometries, velocities of fluid flow, and therefore Re and Nu numbers inside the HE.

2.2 Entropy Generation Minimization approach

It should be noted that the heat transfer and amount of pressure drop are two important factors in the designing process of any thermal systems. It is necessary to consider their impact to reach an optimal condition of the system based on these factors. For this aim, the first law of thermodynamics is not enough because it cannot offer any information about the quality of available energy. The entropy generation is a criterion of irreversibility quantity during a process that is composed of thermal entropy generation (which comprises the irreversibility result in heat transfer) and frictional entropy generations (that indicates irreversibility due to the fluid flow). Consequently, the objective function in the design and optimization processes of the system should be included in both frictional and thermal losses. Thus, the entropy generation should be minimized for the effective parameters to reach a more effective system [46].

By considering the both 1th and 2nd laws of thermodynamics for an element of fluid flowing inside channels of HE with specific heat flux, the following equations could be extracted [29]:

$$\dot{m}dh = q'dx \quad (21)$$

$$d\dot{s}_{gen} = \dot{m}ds - \frac{q'dx}{T + \Delta T/2} \quad (22)$$

where, the parameters \dot{m} , h , q' , x , \dot{s}_{gen} , s , and T denote mass flow rate, specific enthalpy, heat transfer per unit length of the channel, length direction, entropy generation rate, specific entropy, and average flow temperature respectively. By using these equations and the relation of enthalpy and entropy in constant volume, Eq. (23) is expressed [47]:

$$\frac{d\dot{s}_{gen}}{dx} = \dot{s}'_{gen} = \frac{q'dT}{T^2} + \frac{\dot{m}}{\rho T} \left(-\frac{dp}{dx}\right) \quad (23)$$

where, the parameters \dot{s}'_{gen} , p , and ρ represent entropy generation rate per unit length of channel, pressure, and fluid density, respectively.

Finally, the rate of entropy generation per unit length for fluid flowing inside any desired channel could be presented as Eq. (24) [48, 49]:

$$\dot{s}'_{gen,tot} = \frac{q'^2}{4T^2 \cdot \dot{m} \cdot c_p} \cdot \frac{d_{hyd}}{St} + \frac{2\dot{m}^3}{\rho^2 T} \cdot \frac{f}{d_{hyd} \cdot A_{cs}^2} \quad (24)$$

In the last equation, the Stanton number (St), the rate of thermal entropy generation rate per unit length (concerning heat transfer), and the rate of frictional entropy generation rate per unit length (concerning fluid flow) are respectively expressed as Eqs. (25)–(27):

$$St = \frac{q' / \rho \Delta T}{G \cdot c_p} = \frac{Nu}{Re \cdot Pr} \tag{25}$$

$$\dot{s}'_{gen,\Delta T} = \frac{q'^2}{4T^2 \cdot \dot{m} \cdot c_p} \cdot \frac{d_{hyd}}{St} = \frac{q'^2 \cdot d_{hyd} \cdot Pr \cdot Re}{4T^2 \cdot \dot{m} \cdot c_p \cdot Nu} \tag{26}$$

$$\dot{s}'_{gen,\Delta p} = \frac{2\dot{m}^3}{\rho^2 T} \cdot \frac{f}{d_{hyd} \cdot A_{cs}^2} \tag{27}$$

Consequently, the total entropy generation rate per unit length for PPHE with pre-defined geometrical parameters could be rewritten as follows:

$$\dot{s}'_{gen,tot} = \frac{q'^2 \cdot d_{hyd} \cdot Pr}{2T^2 \cdot \mu \cdot c_p \cdot (w_p - 2w_e) \cdot Nu} + \frac{8\dot{m}^3 \cdot f}{\rho^2 T \cdot d_{hyd}^3 \cdot (w_p - 2w_e)^2} \tag{28}$$

For analysing the results in a better shape, the entropy generation can be represented into the dimensionless parameters. Therefore, the following non-dimensional parameters are derived:

$$\varphi = \frac{q'}{k \cdot T} \tag{29}$$

$$\psi = \frac{q' \cdot \rho \cdot \dot{m} \cdot d_{hyd}^2}{\sqrt{KT} \mu^{5/2} \cdot (w_p - 2w_e)^2} \tag{30}$$

So, the non-dimension entropy generation (NDEG) could be expressed as below relations:

$$(NDEG)_{tot} = \frac{\dot{S}_{gen,tot}}{k \varphi^2 \cdot \left(\frac{d_{hyd}}{(w_p - 2w_e)}\right)} \tag{31}$$

$$(NDEG)_{\Delta T} = \frac{1}{2Nu} \tag{32}$$

$$(NDEG)_{\Delta p} = \frac{f \cdot Re^5}{4\psi^2} \tag{33}$$

Also, there are two dimensionless factors, so-called Bejan number (BJN) and ratio of irreversibility issue (ROI). These

criteria are employed to evaluate the thermal and frictional irreversibility portions of the total system irreversibility. Equations (34) and (35) define foresaid dimensionless numbers, respectively [50].

$$BJN = \frac{\dot{s}'_{gen,\Delta T}}{\dot{s}'_{gen,tot}} \tag{34}$$

$$ROI = \frac{\dot{s}'_{gen,\Delta p}}{\dot{s}'_{gen,\Delta T}} \tag{35}$$

As before said, because of the importance of proper performance for HE it is necessary to optimal design of this equipment and its operating conditions. So, a useful criterion as a valid and acceptable indicator is required. Here, a performance evaluation criterion so-called PEC, is employed. The PEC parameter represents the system improvement to reach a better operation in comparison with the base or initial condition. In this study, as PPHE is the novel type of PHE that has been subjected to some geometrical changes to better performance, the PEC parameter is defined proportional to ratio of PPHE to PHE relationships by Eqs. (36) and (37) [51].

$$PEC = \frac{(Nu_{PPHE}) / (Nu_{PHE})}{[(f_{PPHE}) / (f_{PHE})]^{1/3}} \tag{36}$$

$$PEC = \frac{(n_2 Re^{m_2} Pr^{m_3}) / (0.023 Re^{0.8} Pr^{0.4})}{[(n_1 Re^{m_1}) / (0.046 Re^{-0.2})]^{1/3}} \tag{37}$$

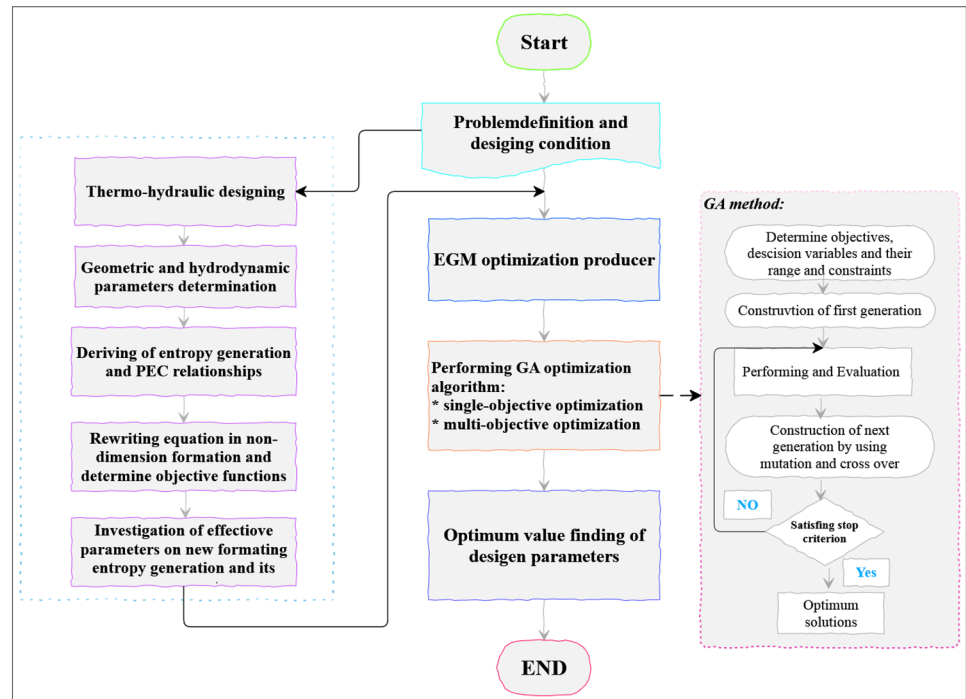
The required air specifications as a working fluid and geometrical data of PPHE are indicated in Table 1.

The solution procedure as shown in the flowchart of Fig. 2, could briefly be summarized as following steps: determining the geometrical parameters and required thermo-hydraulic factors, constructing the entropy generation in relation to effective parameters, defining objective functions according to system design and flow conditions, carrying out sensitive analyze by investigating effects of parameters on objective functions, performing the EGM optimization process, and express the optimal values of decision parameters and optimum points of the system.

Table 1 Required data values of PPHE for simulation process

Parameter	L_p (m)	e (m)	t_w (m)	w_e (m)	Q (kw)	ST (m)
Value	3	0.005	0.001	0.030	150	0.072
Parameter	ρ (kg/m ³)	μ (kg/m.s)	R_f (m ² .K)/W	c_p (kJ/kg.K)	ΔT_{LMTD} (K)	S_L (m)
Value	0.6	0.000041	0.0035	1.04	22	0.042

Fig. 2 Flowchart of the modeling process steps



3 Results and discussion

In this section, the accuracy of the developed model is firstly proven. Afterwards, the effect of several geometrical and operational parameters on the entropy generation rates of the PPHE is presented. In this work, due to the importance of the geometrical effect of PPHE on its performance and flow pattern in PPHE channels, the influence of changing channel height in terms of dimensionless parameter y_i is investigated at different Re numbers. The other studied effective dimensionless parameters are included dimensionless plate width ($w = w_p/L_p$), number of pillow plates (N_p) and Prandtl (Pr) number.

3.1 Model validation

To validate the proposed design modeling, the comparison of the results (thermal and frictional entropy generations) between the outputs of the present work and the results obtained by the reference work is depicted in Fig. 3a. As it could be seen in this figure, there is a good consistency between the results of cases. So that, the average of the relative difference is 1.21% and 0.56% for $(NDEG)_{\Delta T}$ and $(NDEG)_{\Delta p}$, respectively. Also, for a more detailed validation, the result of the change in pressure drop along the channel and variation of the Nu number for different Re numbers are compared with the experimental results by [18] which are presented in Fig. 3b. It reveals that there are 2% and 1.75% relative differences for ΔP and Nu, respectively. It should be noticed that the pressure loss used for the validation was

measured between two measuring ports placed far enough from the inlet and outlet which guaranties considering the fully developed flow region. The experiment was performed over the range of Re numbers 1000 to 8000 and for $Pr=6.0$. Also, to obtain results of Nu number variation, the constant wall heat flux boundary condition is considered because of heating the pillow-plate wall electrically. The geometrical data which used in this validation are listed in Table 2.

3.2 Evaluation of total non-dimension entropy generation

To investigate the influence of PPHE's channel height, plate width, number of pillow plates and Pr number on non-dimensional total entropy generation $(NDEG)_{tot}$, results are depicted for different Re numbers in Figs. 4a to d. These figures display the behavior of $(NDEG)_{tot}$ for changing above mentioned variables that for each value of them, there is a specific Re number as an optimum Re in which minimum entropy generation happens and vice versa. As shown in Fig. 4a, the minimum of $(NDEG)_{tot}$, for example, for $y_i = 0.04$ is about 0.027 and occurs at $Re = 2500$. However, this minimum value of $(NDEG)_{tot}$ becomes smaller by increasing y_i and the corresponding amount of the Re (i.e. optimum Re number) is grown, although large channel height is not really applicable. Obviously, the efficiency of the system is improved when the entropy generation and exergy loss are minimized. Consequently, a high y_i value is required for an optimal operation which leads to decrease the pressure drop of

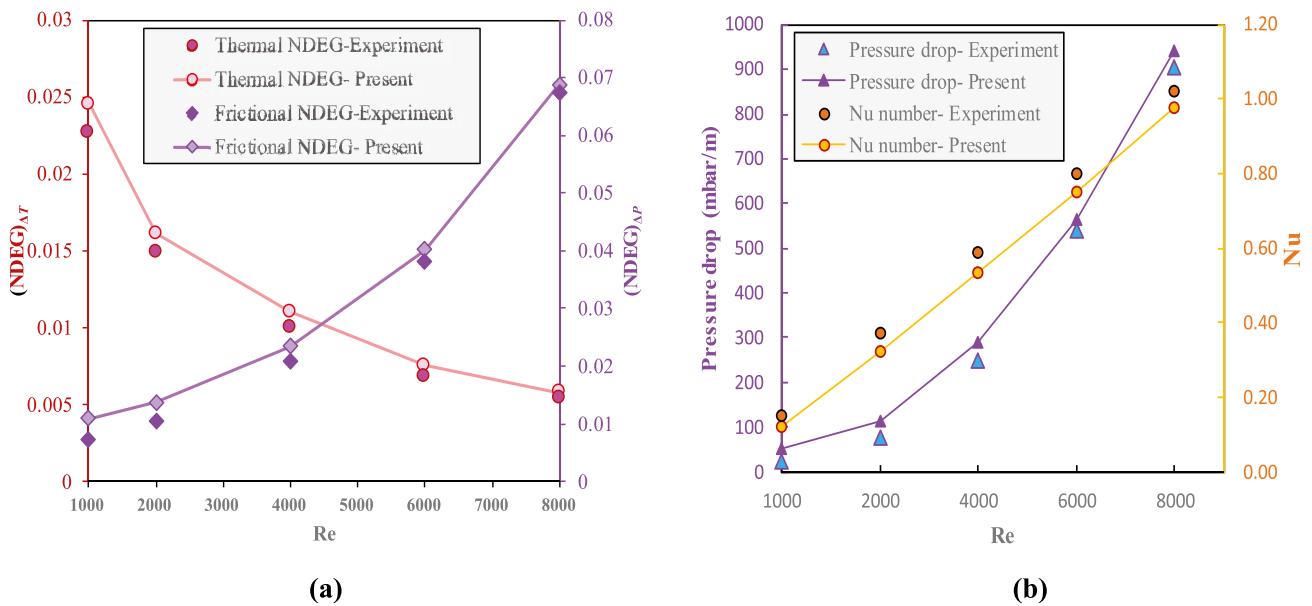


Fig. 3 Comparison between the outputs of the present work and experimental data obtained from [18], **a** thermal and frictional non-dimension entropy generations, **b** pressure drop and Nusselt number

the HE. On the contrary, increasing channel height in terms of y_i would significantly debilitate the coefficient of heat transfer. Thus, according to the second law of thermodynamics, it is required to identify optimal y_i and Re number which is affected by mass flow rate. This matter will discuss later. Figure 4b illustrates the effect of dimensionless plate width (w) at different Re number on the $(NDEG)_{tot}$ that both minimum value of it and optimum Re are increased by rising w . This figure shows the direct relation between $(NDEG)_{tot}$ and w at a constant Re number. The variation of $(NDEG)_{tot}$ by changing the number of pillow plates is presented in Fig. 4c. It shows the lowest values of $(NDEG)_{tot}$ for $N_p = 50$ to $N_p = 70$ has a descending trend and this minimum of $(NDEG)_{tot}$ will be disappeared in upper amounts of N_p . Also, the optimum Re number is increased by increments of N_p . Figure 4d depicts the influence of Pr number on $(NDEG)_{tot}$ by variation of Re number. According to this figure, there is a minimum value for $(NDEG)_{tot}$ corresponding to the certain optimum Re at any Pr that has an indirect relation with Pr.

Table 2 The geometrical design parameters of the reference work [18]

Parameter	S_T	S_L	d_{sp}	e_i	t_w
Value (mm)	42	36	10	3.0	1.0

3.3 Evaluation of thermal and frictional entropy generation

Figure 5a–c illustrate the effect of some influenced geometrical variables as well as Fig. 5d shows Pr effect on the non-dimension thermal and frictional entropy generations for different Re numbers. As for these figures, the $(NDEG)_{ΔP}$ rises and $(NDEG)_{ΔT}$ reduces by increasing y_i , w , N_p , and Pr because of the direct relation of frictional entropy generation with f and the inverse relation of thermal entropy generation with Nu number. Also, it is found that there is a conflicting behavior of $(NDEG)_{ΔT}$ and $(NDEG)_{ΔP}$ by varying Re number for each certain investigated parameter. For example in Fig. 5a, the amount of $(NDEG)_{ΔT}$ and $(NDEG)_{ΔP}$ for $Re = 3100, 4300$ are 0.016, 0.01 and 0.013, 0.022, respectively. This figure shows at any Re, $(NDEG)_{ΔT}$ and $(NDEG)_{ΔP}$ become lower by increasing y_i . The inverse relation is observed in Fig. 5b and c between $(NDEG)_{ΔT}$ and $(NDEG)_{ΔP}$ at specific Re by advancing w and N_p , respectively. In this way, Fig. 5d demonstrates the role of Pr on parts of entropy generation that at a particular Re, $(NDEG)_{ΔT}$ is reduced and $(NDEG)_{ΔP}$ is grown by rising Pr.

3.4 Evaluation of Bejan number

The Bejan number (BJN), according to Eq. (34), is a defined parameter to specify the amount of thermal entropy generation to the total entropy generation. Figures 6a to d are

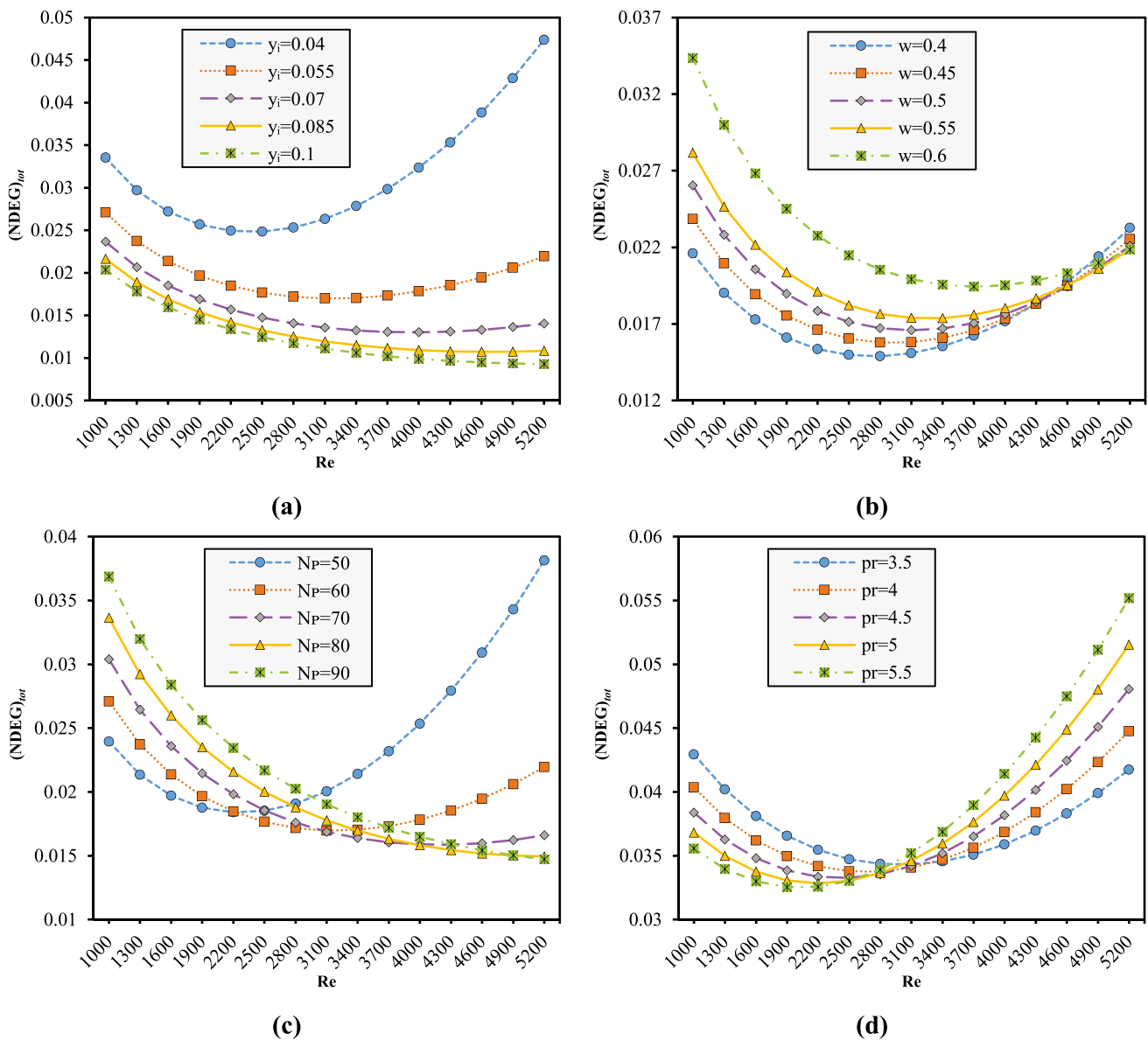


Fig. 4 Variation of non-dimensional total entropy generation of PPHE at different Re numbers by changing, **a** dimensionless channel height, **b** dimensionless plate width, **c** pillow plate numbers, and **d** Prandtl number

depicted to analyze the influence of geometrical parameters of the PPHE and Pr number on BJN. Figure 6a shows the effect of y_i on BJN for varying Re that this dimensionless parameter is raised by increasing y_i at any Re which could be described by increasing the rate of heat transfer in higher y_i values and so smaller amount of $(NDEG)_{\Delta T}$. On the other hand, increasing Re number and entering to turbulence regime of the stream leads to formation of recirculation zones and increasing Nu number and heat transfer,

consequently. However, smaller recirculation zones are resulted by increasing channel height or hydraulic diameter which they limited to the near wall region. It could also be seen in [17, 18]. This means that the Nu number increases intensely in high Re numbers with an increase in the channel height and hydraulic diameter. It could be exacerbated the difference between the columns at the higher Re number in Fig. 6. Also, another result of reduction in the recirculation zone affected area is the decreases in pressure drop as

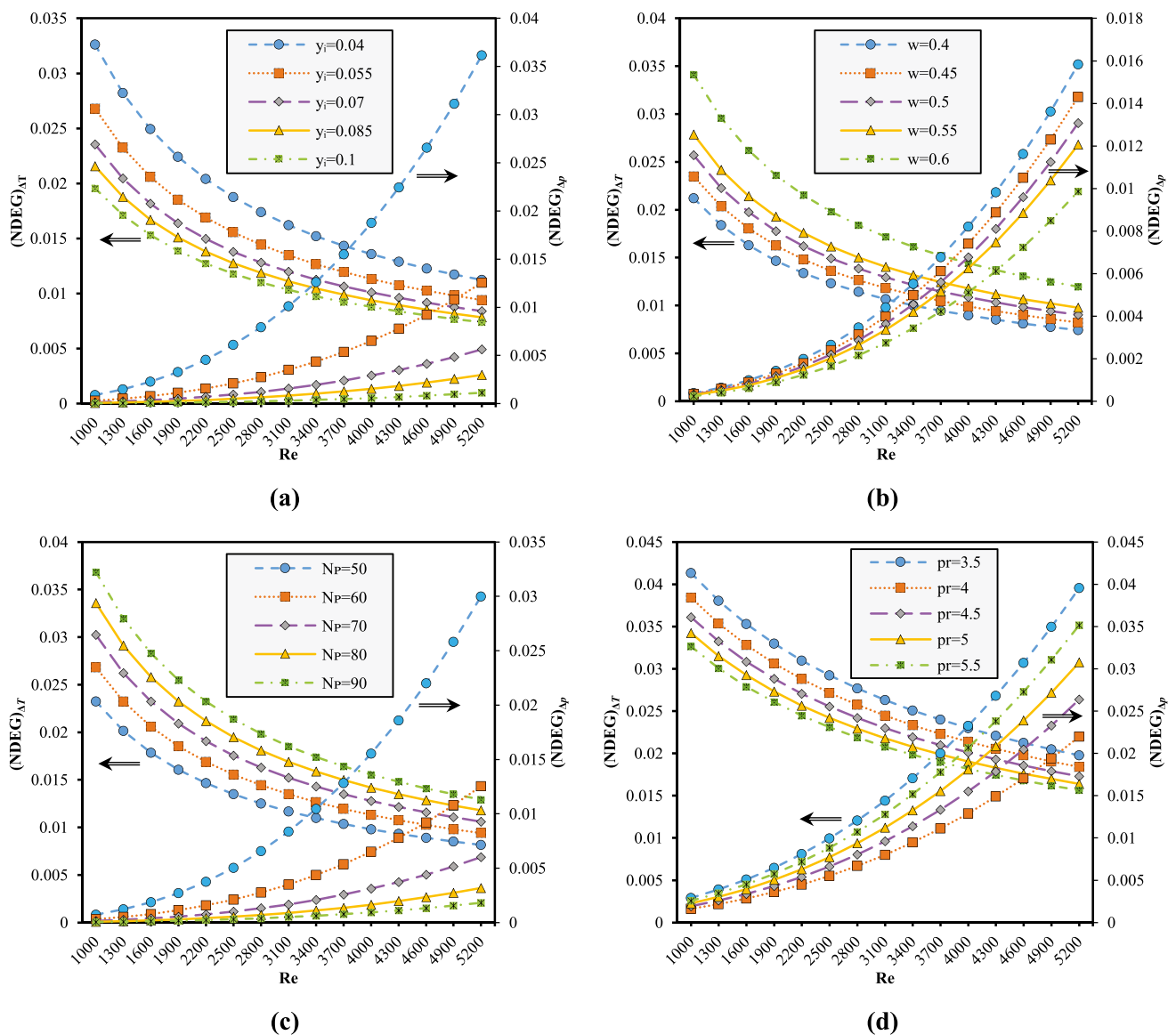


Fig. 5 Variation of non-dimensional thermal (left) and frictional (right) entropy generation of PPHE at different Re number by changing, **a** dimensionless channel height, **b** dimensionless plate width, **c** pillow plate numbers, and **d** Pr number

the channel height y_i or N_p increases which could amplify difference between the columns of BJN at the higher Re. The change of BJN for different w and N_p values by varying Re is illustrated in Fig. 6b and c that has a same behavior as the previous figure. It could be deduced from these figures, increasing heat transfer due to growing heat transfer area by augmenting of w and N_p causes decreasing BJN. For instance, in Fig. 6b, the BJN advances from

0.5 to 0.68 by increasing w from 0.4 to 0.6 at $Re = 4000$. In this way in Fig. 6c, the BJN reduces from 0.8 to 0.4 for $Re = 2200$ to 4000 at $N_p = 60$. It is obvious that an increase in the BJN at any w or N_p is more noticeable in higher Re. Ultimately, Fig. 6d shows the conflict trend between Pr and BJN in all Re numbers by which could be interpreted by a direct and inverse relation between Pr and Nu and Nu and BJN, respectively.

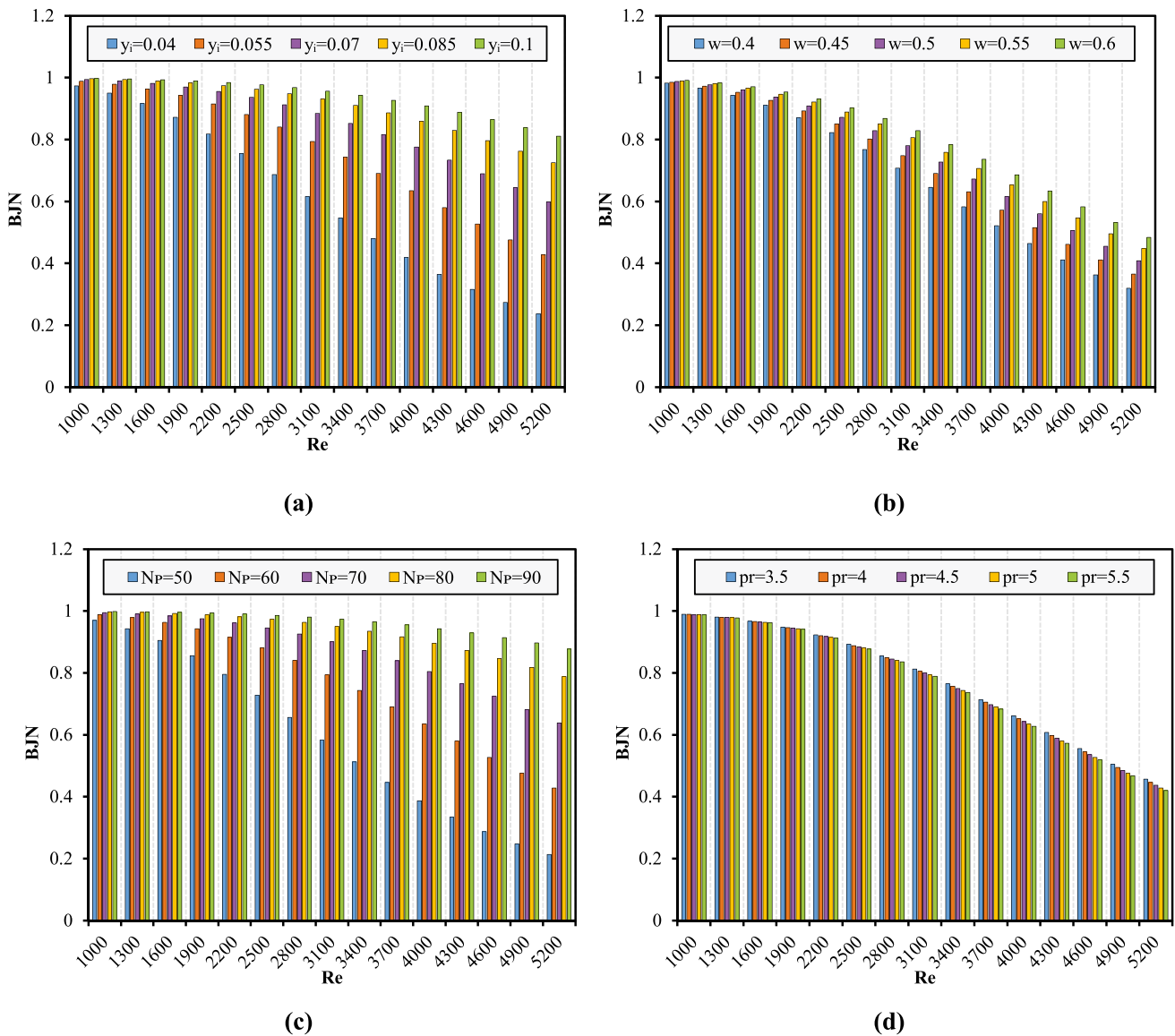


Fig. 6 The variation of Bejan number of PPHE at different Re numbers by changing, **a** dimensionless channel height, **b** dimensionless plate width, **c** pillow plate numbers, and **d** Prandtl number

3.5 Evaluation the rate of irreversibility

Another beneficial parameter in EGM analysis is the rate of irreversibility (ROI) that defined as a ratio of frictional to thermal entropy generation and is depicted in Fig. 7a to d with the variation of y_i , w , N_p , and Pr at various Re. As it can be seen in Fig. 7a to c, the ROI parameter reduces by advancing in values of PPHE geometrical variables at any Re which presents decreasing the contribution of $(NDEG)_{\Delta p}$ versus $(NDEG)_{\Delta T}$. Also, it is found that ROI increases by augmentation Re number which this trend is more intense in lower values of geometrical parameters. This demonstrates the domination of $(NDEG)_{\Delta T}$

to $(NDEG)_{\Delta p}$ at low Re numbers and $(NDEG)_{\Delta p}$ to $(NDEG)_{\Delta T}$ for high Re numbers that should be considered in designing HE corresponding to the range of operation. Figure 7d illustrates the compatible behavior of Pr and ROI that by growing Pr at any Re, the higher values of ROI can be attained and role of $(NDEG)_{\Delta p}$ would be more significant. The similar differences between the results at the higher Re number have been seen in Fig. 7 which could be justified like what is mentioned for Fig. 6.

Here, it could be beneficial to compare the obtained PPHE performance result with the conventional flat plate heat exchanger (FPHE) at different Re numbers. So, details of this comparison are presented Appendix A.

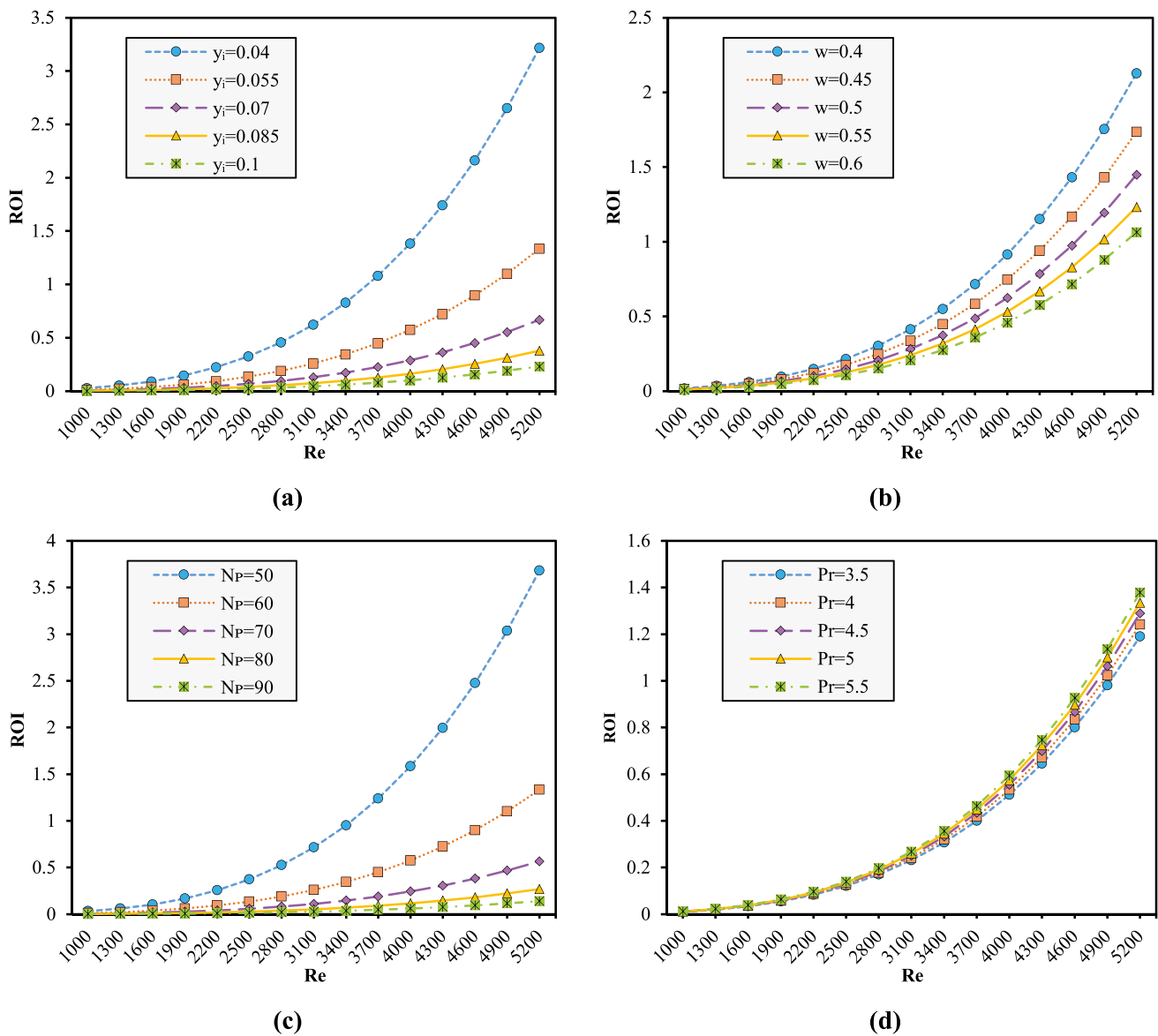


Fig. 7 Variation of irreversibility rate of PPHE at different Re numbers by changing, **a** dimensionless channel height, **b** dimensionless plate width, **c** pillow plate numbers, and **d** Prandtl number

3.6 Performance evaluation criteria

According to previous outline, PEC is a parameter to indicate the improvement in a system to achieve the better performance and higher efficiency. Figures 8 and 9 reveal the variation of PEC of PPHE with different Re. The influence of channel height in terms of y_i on PEC is depicted in Fig. 8. As before said, increase in y_i leads the increase the Nu and pressure drop in investigated PPHE which Nu augmentation

is stronger than pressure drop due to power of 1/3 for friction factor in PEC equation. Hence, PEC criterion has the higher value by growing y_i at any particular Re. Also, Fig. 8 shows PPHE performance is acceptable in y_i values upper than 0.04 to about $y_i = 0.085$ which higher y_i values have not significant effect or negative consequence. Also, it is seen that the PEC behavior depends on the flow regime and is increased by augmenting the Re for each y_i . This could be described by the fact that Nu is much higher in

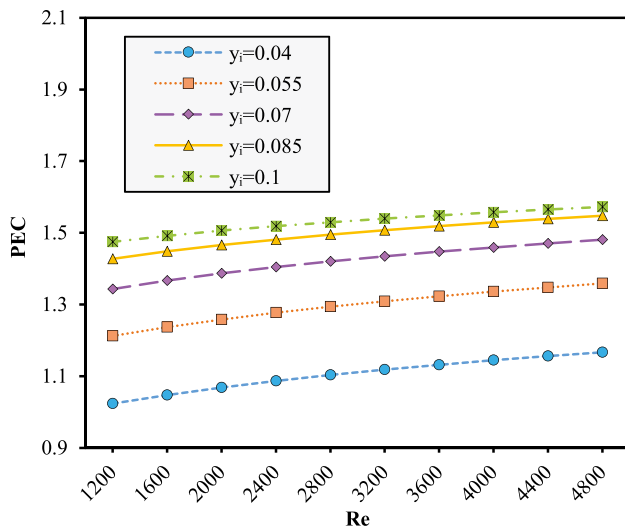


Fig. 8 Variation of performance evaluation criterion by changing dimensionless channel height at different Reynolds numbers

turbulent flow stream than laminar and better values of Nu ratio in PEC equation can be achieved by using heat transfer increasing techniques. Furthermore, turbulent regime's friction factor is lower than of the laminar flow.

The change of PEC with w , as another PPHE geometrical parameter, is illustrated in Fig. 9. This figure reveals that high PEC amounts occur in advance Re numbers for various w because of increase the Nu and heat transfer for higher Re values. On the other hand, the increasing cross

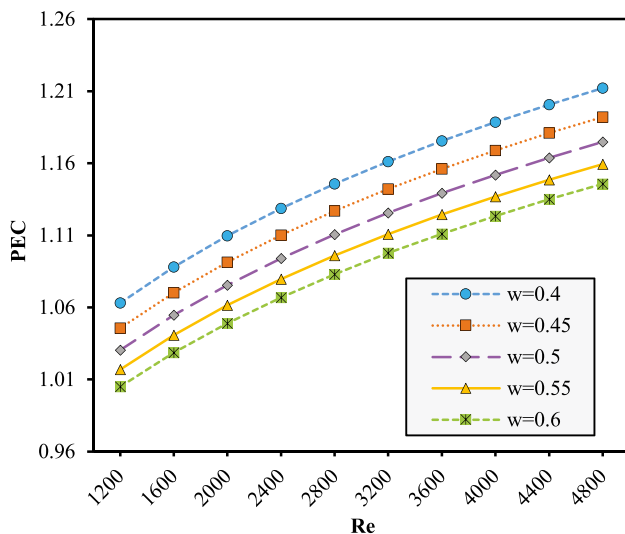


Fig. 9 Variation of performance evaluation criterion by changing dimensionless plate width at different Reynolds numbers

sectional area of PPHE channel is another consequence of bigger plate with of w . So, the Nu and f of PPHE would be decreased and lower PEC values are resulted in any Re number as shown in Fig. 9.

3.7 Optimization procedure

3.7.1 Single-objective optimization

An optimization in form of single-objective is individually applied for each objective function in the investigated range for each of the effective decision variables. Here, $(NDEG)_{tot}$ and PEC are investigated as two objective functions which should be minimized and maximized, respectively. Selecting the best individual for each generation in the evolution process is done by applying optimization using a genetic algorithm (GA) which considers the fitness function values of every individual. In this way, the design parameters of PPHE such as the plate width, pillow height, number of pillow plates, and Re number are used as decision variables. Performing single-objective optimization (SOO), Figs. 10a and b show variations of these functions with respect to the number of generations that have converged to the best value of them. Finally, the corresponding optimum values of $(NDEG)_{tot}$ and PEC and decision variables are obtained according to Table 3. It is worth mentioning that in this table, the $(NDEG)_{tot}$ and PEC are respectively considered the objective functions in SOO₁ and SOO₂.

3.7.2 Multi-objective optimization

A multi-objective optimization (MOO) problem is a procedure with simultaneous optimizing two or more objective functions with different constraints. This procedure usually expresses a probably uncountable set of solutions to evaluate vectors to reach the best possible trade-offs. In other words, each objective function gives a vector including the set of objective values corresponding to the primary objectives to be optimized [52–54].

Moreover, to obtain a suitable balance between the objectives and perform complete exploration for the determined tradeoffs range within the space of objective, the multi-objective GA is utilized to solve this MOO problem. Thus, it causes to find a set of solutions that indicate the best relationship between the two objective functions. The Pareto optimal front is employed to illustrate the relationship between results of MOO in order to specify the best possible solution among obtained ones [55, 56]. The notable tip is that all of the points on the Pareto frontier could be considered as an

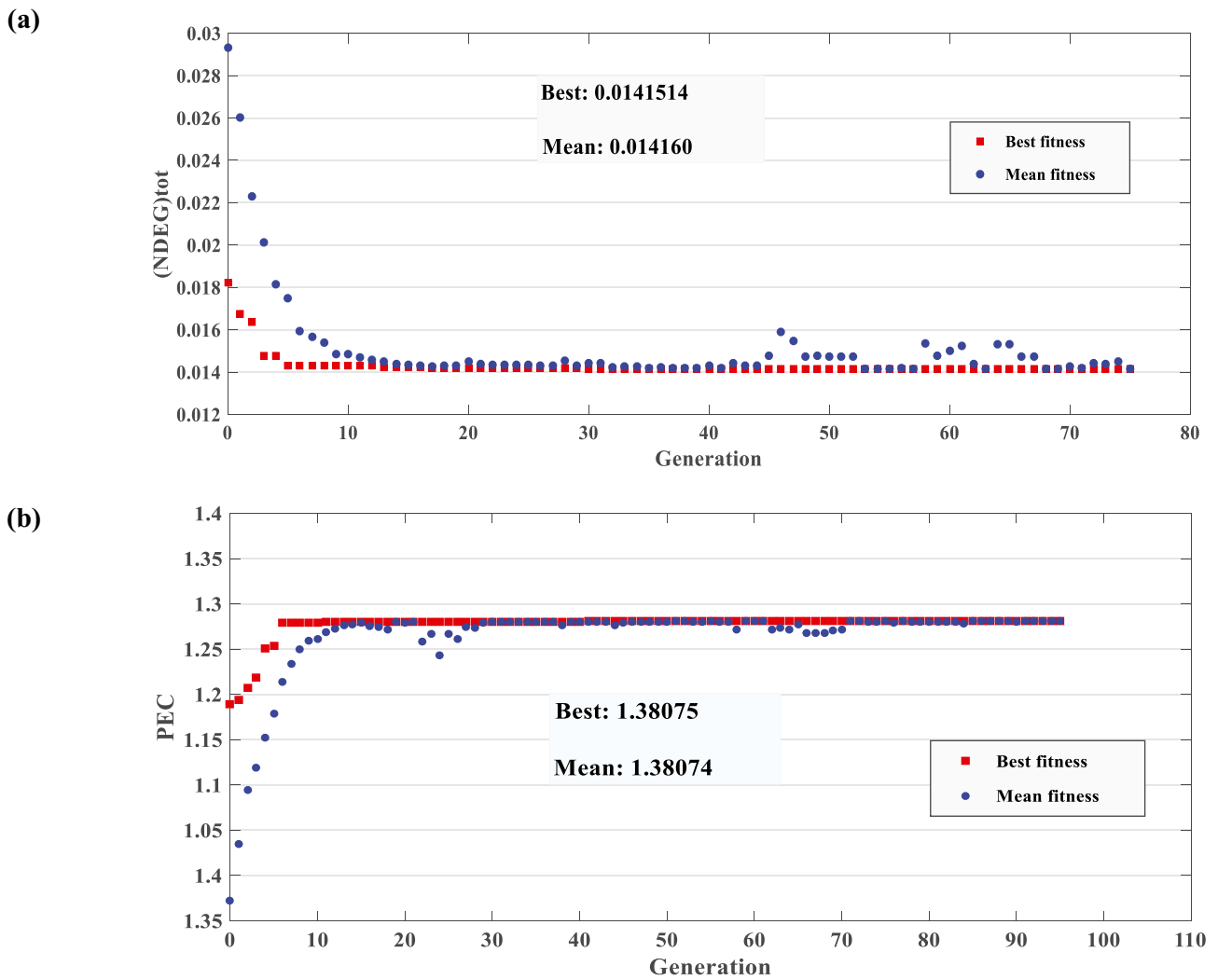


Fig. 10 Single-objective optimization convergence to the optimum value for, **a** non-dimensional total entropy generation and **b** performance evaluation criterion

optimal point candidate, which the designer should select one point based on the desirable design conditions and limitations. This process is done by applying a decision-making approach. Taking into account previous works in the field, the LINMAP decision-making approach could be considered a reliable approach that is based on the minimum distance from the ideal point on the Pareto frontier [57, 58].

Firstly in this study, for better recognizing and designing of the system the criteria of $(NDEG)_{\Delta T}$ and $(NDEG)_{\Delta p}$ are

used for simultaneous optimization because of their conflicting behavior. Figure 11 represents the Pareto front obtained by performing the MOO producer that leftmost point of this curve reveals that $(NDEG)_{\Delta p}$ has its minimum value, while $(NDEG)_{\Delta T}$ reaches its maximum amount. This figure indicates the conflicting behavior of the MOO solutions which exists between the thermal and frictional entropy generations as irreversible losses. As a result, the entropy generation due to fluid friction is not negligible in the MOO procedure

Table 3 Single-objective optimization results and optimum value of variables

Objective functions/ Decision variables	$(NDEG)_{tot}$	PEC	y_i	w	N_p	Re
Range	---	---	0.04–0.1	0.4–0.8	50–100	1000–5000
Optimum value in SOO ₁	0.01416	---	0.067	0.63	78	3100
Optimum value in SOO ₂	---	1.3807	0.054	0.58	66	3700

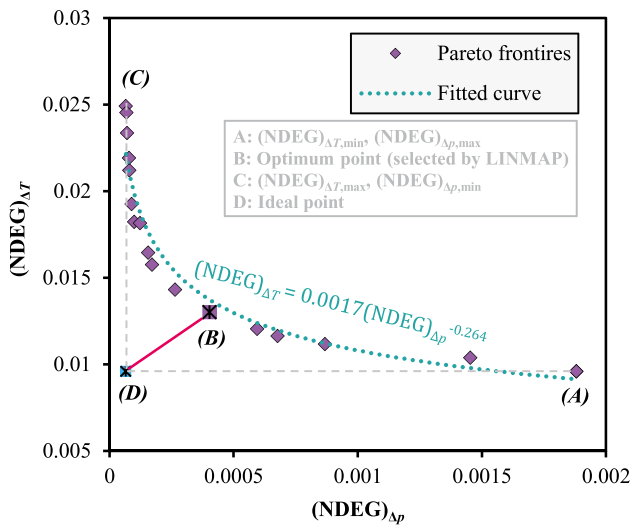


Fig. 11 The Pareto-optimal front for MOO₁ using NSGA-II (objective functions: non-dimensional thermal and frictional entropy generations)

and plays an important role in characterize the optimal solutions. It should be noted that the relationship between the optimal values of the two objective functions (i.e. $(NDEG)_{\Delta T}$ and $(NDEG)_{\Delta p}$) for all optimal solutions located on the discussed Pareto front can be derived by curve fitting which is denoted in Fig. 11. It is beneficial to say that R^2 factor is a criterion to evaluate the accuracy of the developed equation that here is $R^2 = 0.959$ indicating the acceptable accuracy of the fitted curve.

As a main step of MOO in the present study, by attention to the role of PEC and $(NDEG)_{tot}$ as the two important factors in PPHE evaluation which have an adversely behavior, it could be advantageous to consider them as the objective functions in MOO₂ process to find the optimal values of system variables. Figure 12 illustrates the result for Pareto-optimal front and the trade-off between its two objective functions, i.e., $(NDEG)_{tot}$ as the horizontal axis

Table 4 Coefficients of the optimal PEC- $(NDEG)_{tot}$ fitted correlation

Constant	<i>a</i>	<i>b</i>	<i>c</i>	<i>d</i>
Value	6×10^7	-3×10^6	39,398	- 191.89

Table 5 Multi-objective optimization results and optimum value of variables

MOO₁	$[(NDEG)_{\Delta T}]_{opt}$	$[(NDEG)_{\Delta p}]_{opt}$	$(y_i)_{opt}$	$(w)_{opt}$	$(N_p)_{opt}$	$(Re)_{opt}$
	0.0130091	0.000404	0.051	0.43	57	4425
MOO₂	$[(NDEG)_{tot}]_{opt}$	$(PEC)_{opt}$	$(y_i)_{opt}$	$(w)_{opt}$	$(N_p)_{opt}$	$(Re)_{opt}$
	0.014502	1.3712	0.059	0.62	69	3265

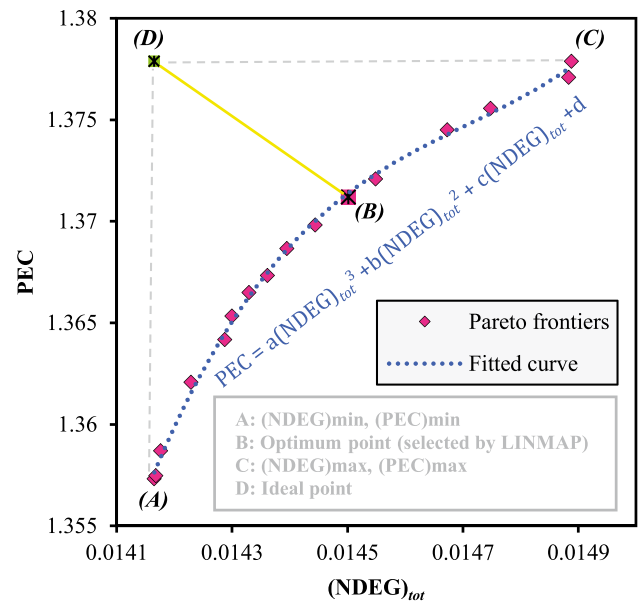


Fig. 12 The Pareto-optimal front for MOO₂ using NSGA-II (objective functions: PEC and non- dimensional total entropy generation)

and the performance evaluation criteria as the vertical axis. In this figure, the ideal or best point *D* shows the highest value of PEC and lowest amount of $(NDEG)_{tot}$. However, due to pint *D* is really unavailable, the optimum point of *B* can be specified by LINMAP method that considers the minimum distance to the point *D* Point among other optimum points on the Pareto curve. It can be seen that by any changing of geometrical variables which reduces the total entropy generation, the PEC is increased and vice versa although, each point on the Pareto front represent the optimal value, naturally.

The relationship between the optimal values of PEC and $(NDEG)_{tot}$ could be derived by curve fitting in form of a third-order polynomial equation that presented in Fig. 12.

The constants of this correlation are expressed in Table 4. It is beneficial to say that R^2 factor is a criterion to evaluate the accuracy of developed equation that here is $R^2 = 0.998$ indicating the high accuracy of fitted curve.

As the final results of the MOO procedure, the optimum values of the objective functions and decision variables are tabulated in Table 5.

4 Conclusion

In this study, the optimal analysis of pillow plate HE based on the second law of thermodynamics and EGM, as well as its thermo-hydraulic modeling, includes the heat transfer and fluid flow characteristics were investigated. As expected, thermo-hydraulic results indicated a good performance which could be due to the wavy shape of the pillow-plate channels on the flow condition and useful turbulence in flow streams. By deriving non-dimensioned parameters, the influence of several geometric parameters such as longitudinal and transverse pitch, channel height, and diameter of the weld spot of PPHE were considered for a wide range of Reynolds numbers. It was found out that for each geometrical variable include the channel height of PPHE, plate width, number of pillow plates, and Pr number, there was a particular Re number in which minimum entropy generation occurred. For example, for the dimensionless channel height $y_i=0.04$, minimum total entropy generation was equal to 0.027 and happened at $Re=2500$. Also, results illustrated that amount of $(NDEG)_{tot}$ decreased by increasing the y_i , as well as, there was a conflicting behavior of $(NDEG)_{\Delta T}$ and $(NDEG)_{\Delta p}$ by varying Re number at any channel height. For instance, at $y_i=0.06$ the amount of $(NDEG)_{\Delta T}$ and $(NDEG)_{\Delta p}$ for $Re=3100, 4300$ were 0.017, 0.08 and 0.013, 0.021, respectively. For completing analyzing of EGM for PPHE, the behaviors of BJN and ROI as the two other beneficial EGM parameters were investigated for different model variables and Re numbers.

For finding the optimal condition of system design, the considered objective functions were taken into account by applying the GA optimization approach in the form of SOO

and MOO and the optimum PPHE dimensionless design variables of channel height, plate width, number of pillow plate, and Re number were obtained. In this research, the PEC was introduced and used as the objective function and it optimized against the $(NDEG)_{tot}$. The obtained Pareto optimal front showed the conflicting behavior between PEC and $(NDEG)_{tot}$ that increment of PEC was required to increase in $(NDEG)_{tot}$ and hence, the optimal value of them by LINMAP decision-making method was achieved and their correlation was derived. Considering the PEC and $(NDEG)_{tot}$ as two objective-functions in a MOO procedure, the final optimum values of the objective functions were obtained as $PEC_{opt}=1.3712$ and $(NDEG)_{tot,opt}=0.0145$ which occurred at $Re=3265$.

Appendix

This appendix deals with the general comparison of PPHE and conventional FPHE modeling result. In this way, the FPHE model with similar dimensions of PPHE has been developed using particular hydraulic diameter and correlations of f and Nu as follows [59]:

$$d_{hyd} = 2e_i \tag{A1}$$

$$f = 3.44 Re^{-0.225} \tag{A2}$$

$$Nu = 0.143 Re^{0.71} Pr^{0.3} \tag{A3}$$

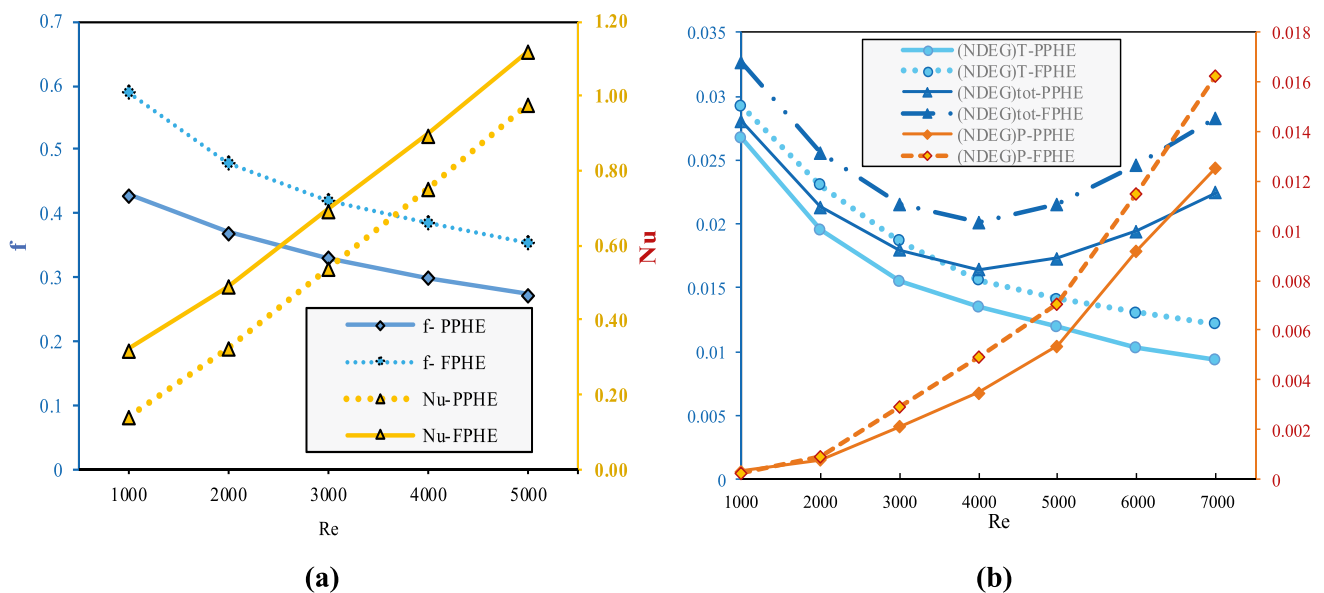


Fig. 13 Comparison of PPHE and FPHE at different Re numbers, **a** changing friction factor and Nu, **b** changing $(NDEG)_{tot}$, $(NDEG)_{\Delta T}$ and $(NDEG)_{\Delta p}$

Based on the above equations, to observe the f and Nu trends as the evaluating parameters by varying Re , results of the developing numerical code for the FPHE are compared with the PPHE. This comparison is depicted in Fig. 13.

It could be seen in Fig. 13(a) that friction factor and heat transfer of PPHE are lower and higher than FPHE, respectively. By attention to the structure of PPHE and consequent redirected flow around the welding spots inside the channel, formation of boundary layer leads to improve the heat transfer comparison to FPHE. However, this could slightly increase the pressure drop in PPHE channel depending on welding points pattern and their distances. Fig. 13(b) illustrates variation of main EGM assessment parameters i.e. $(NDEG)_{tot}$, $(NDEG)_{\Delta T}$ and $(NDEG)_{\Delta p}$ in different Re numbers for both PPHE and FPHE. As expected, because of some PPHE structural features against the FPHE which have been led to improve heat transfer and totally reduction in pressure drop, the derived thermal, frictional and total form of non-dimensional entropy generation in PPHE are lower than FPHE.

Declarations

Conflict of interest We would like to say that we and our institution don't have any conflict of interest and don't have any financial or other relationship with other people or organizations that may inappropriately influence the author's work.

References

- Ebrahimi-Moghadam A, Farzaneh-Gord M (2023) A sustainable optimal biomass waste-driven CCHP system to boost the nearly zero energy building concept. *Energy Convers Manag* 277:116669. <https://doi.org/10.1016/j.enconman.2023.116669>
- Bai B, Zhou R, Yang G et al (2023) The constitutive behavior and dissociation effect of hydrate-bearing sediment within a granular thermodynamic framework. *Ocean Eng* 268:113408. <https://doi.org/10.1016/j.oceaneng.2022.113408>
- Chen L-Q, Zhao Y (2022) From classical thermodynamics to phase-field method. *Prog Mater Sci* 124:100868. <https://doi.org/10.1016/j.pmatsci.2021.100868>
- Luo H, Lou Y, He K, Jiang Z (2023) Coupling in-situ synchrotron X-ray radiography and FT-IR spectroscopy reveal thermally-induced subsurface microstructure evolution of solid propellants. *Combust Flame* 249:112609. <https://doi.org/10.1016/j.combustflame.2022.112609>
- Fang JX, Wang JX, Wang YJ et al (2022) Microstructure evolution and deformation behavior during stretching of a compositionally inhomogeneous TWIP-TRIP cantor-like alloy by laser powder deposition. *Mater Sci Eng A* 847:143319. <https://doi.org/10.1016/j.msea.2022.143319>
- Herrera B, Gallego A, Cacia K (2021) Experimental evaluation of a thermosiphon-based heat exchanger working with a graphene oxide (GO) nanofluid in a cogeneration system. *Therm Sci Eng Prog* 24:100949
- Jassim EI, Ahmed F (2021) Assessment of nanofluid on the performance and energy-environment interaction of Plate-Type-Heat Exchanger. *Therm Sci Eng Prog* 100988
- Rong G, Cheng M, Sheng Z et al (2022) Investigation of counter-rotating shock wave and wave direction control of hollow rotating detonation engine with Laval nozzle. *Phys Fluids* 34:56104. <https://doi.org/10.1063/5.0089207>
- Tran JM, Linnemann M, Piper M, Kenig EY (2017) On the coupled condensation-evaporation in pillow-plate condensers: Investigation of cooling medium evaporation. *Appl Therm Eng* 124:1471–1480. <https://doi.org/10.1016/j.applthermaleng.2017.06.050>
- Guo Y, Qiu C, Xu M et al (2021) Crack failure analysis of laser 316L stainless steel edge joints in pillow plate heat exchanger used in oil refinery. *Eng Fail Anal* 122:105215
- Yao Y, Ding J, Zhang Y et al (2022) Heat transfer performance of pillow plate heat exchanger with molten salt and supercritical carbon dioxide. *Int J Heat Mass Transf* 183:122211
- Selvnes H, Allouche Y, Hafner A (2021) Experimental characterisation of a cold thermal energy storage unit with a pillow-plate heat exchanger design. *Appl Therm Eng* 199:117507
- Goedecke R, Scholl S (2019) Modelling and simulation of a pillow plate thermosiphon reboiler. *Heat Mass Transf* 55:95–104
- Scholl S (2018) Pillow plate heat exchangers as falling film evaporator or thermosiphon reboiler. In: *Innovative Heat Exchangers*. Springer, pp 267–294
- Dormohammadi R, Farzaneh-Gord M, Ebrahimi-Moghadam A, Ahmadi MH (2018) Heat transfer and entropy generation of the nanofluid flow inside sinusoidal wavy channels. *J Mol Liq* 269:229–240. <https://doi.org/10.1016/j.molliq.2018.07.119>
- Arsenyeva O, Tran J, Piper M, Kenig E (2019) An approach for pillow plate heat exchangers design for single-phase applications. *Appl Therm Eng* 147:579–591. <https://doi.org/10.1016/j.applthermaleng.2018.08.083>
- Piper M, Tran JM, Kenig EY (2015) CFD Study of Fluid Dynamics and Heat Transfer for Single-Phase Flow in the Wavy Channel Between Pillow Plates. *Chemie Ing Tech* 87:216–225
- Piper M, Zibart A, Tran JM, Kenig EY (2016) Numerical investigation of turbulent forced convection heat transfer in pillow plates. *Int J Heat Mass Transf* 94:516–527
- Tran JM, Piper M, Kenig EY (2015) Experimental Investigation of Convective Heat Transfer and Pressure Drop in Pillow Plates under Single-Phase Through-Flow Conditions. *Chemie Ing Tech* 87:226–234
- Tran JM, Sommerfeld S, Piper M, Kenig EY (2015) Investigation of pillow-plate condensers for the application in distillation columns. *Chem Eng Res Des* 99:67–74
- Mitrovic J, Peterson R (2007) Vapor condensation heat transfer in a thermoplate heat exchanger. *Chem Eng Technol Ind Chem Equipment-Process Eng* 30:907–919
- Piper M, Olenberg A, Tran JM, Kenig EY (2015) Determination of the geometric design parameters of pillow-plate heat exchangers. *Appl Therm Eng* 91:1168–1175
- Mitrovic J, Maletic B (2011) Numerical simulation of fluid flow and heat transfer in thermoplates. *Chem Eng Technol* 34:1439–1448
- Xie GN, Sundén B, Wang QW (2008) Optimization of compact heat exchangers by a genetic algorithm. *Appl Therm Eng* 28:895–906
- Alizadeh M, Ganji DD (2021) Heat transfer characteristics and optimization of the efficiency and thermal resistance of a finned thermosiphon. *Appl Therm Eng* 183:116136

26. Alizadeh M, Nabizadeh A, Fazlollahtabar A, Ganji DD (2021) An optimization study of solidification procedure in a wavy-wall storage unit considering the impacts of NEPCM and curved fin. *Int Commun Heat Mass Transf* 124:105249
27. de Araújo ÉF, Ribeiro GB, Guimarães LNF (2020) Design optimization of a cross-flow He-Xe recuperator through second law analysis. *Therm Sci Eng Prog* 19:100568
28. Bezaatpour M, Rostamzadeh H (2020) Energetic and exergetic performance enhancement of heat exchangers via simultaneous use of nanofluid and magnetic swirling flow: A two-phase approach. *Therm Sci Eng Prog* 20:100706
29. Bejan A (1977) The concept of irreversibility in heat exchanger design: counterflow heat exchangers for gas-to-gas applications
30. Zhou Y, Zhu L, Yu J, Li Y (2014) Optimization of plate-fin heat exchangers by minimizing specific entropy generation rate. *Int J Heat Mass Transf* 78:942–946. <https://doi.org/10.1016/j.ijheatmasstransfer.2014.07.053>
31. Farzaneh-Gord M, Ameri H, Arabkoohsar A (2016) Tube-in-tube helical heat exchangers performance optimization by entropy generation minimization approach. *Appl Therm Eng* 108:1279–1287
32. Sodagar-Abardeh J, Ebrahimi-Moghadam A, Farzaneh-Gord M, Norouzi A (2020) Optimizing chevron plate heat exchangers based on the second law of thermodynamics and genetic algorithm. *J Therm Anal Calorim* 139:3563–3576. <https://doi.org/10.1007/s10973-019-08742-3>
33. Guo J, Cheng L, Xu M (2010) Multi-Objective Optimization of Heat Exchanger Design by Entropy Generation Minimization. *J Heat Transfer* 132:81801–81808
34. Shi Z, Dong T (2014) Thermodynamic investigation and optimization of laminar forced convection in a rotating helical tube heat exchanger. *Energy Convers Manag* 86:399–409
35. Leong KY, Saidur R, Khairulmaini M et al (2012) Heat transfer and entropy analysis of three different types of heat exchangers operated with nanofluids. *Int Commun Heat Mass Transf* 39:838–843
36. Ebrahimi-Moghadam A, Moghadam AJ (2019) Optimal design of geometrical parameters and flow characteristics for Al₂O₃/water nanofluid inside corrugated heat exchangers by using entropy generation minimization and genetic algorithm methods. *Appl Therm Eng* 149:889–898. <https://doi.org/10.1016/j.applthermaleng.2018.12.068>
37. Deymi-Dashtebayaz M, Akhouni M, Ebrahimi-Moghadam A et al (2020) Thermo-hydraulic analysis and optimization of CuO/water nanofluid inside helically dimpled heat exchangers. *J Therm Anal Calorim*. <https://doi.org/10.1007/s10973-020-09398-0>
38. Rostami AK, Alizadeh M, Fazlollahtabar A, Ganji DD (2021) Performance enhancement of a maple leaf-shaped latent heat energy storage unit by adding nanoparticles and leaf vein fins. *J Energy Storage* 43:103159
39. Alizadeh M, Shahavi MH, Ganji DD (2022) Performance enhancement of nano PCM solidification in a hexagonal storage unit with innovative fin shapes dealing with time-dependent boundary conditions. *Energy Rep* 8:8200–8214
40. Kotcioglu I, Caliskan S, Cansiz A, Baskaya S (2010) Second law analysis and heat transfer in a cross-flow heat exchanger with a new winglet-type vortex generator. *Energy* 35:3686–3695
41. Yousefi M, Darus AN, Mohammadi H (2011) Second law based optimization of a plate fin heat exchanger using Imperialist Competitive Algorithm. *Int J Phys Sci* 6:4749–4759
42. Alizadeh M, Ganji DD (2020) Multi-objective optimization of an externally finned two-phase closed thermosyphon using response surface methodology. *Appl Therm Eng* 171:115008
43. Ebrahimi-Moghadam A, Mohseni-Gharyehsafa B, Farzaneh-Gord M (2018) Using artificial neural network and quadratic algorithm for minimizing entropy generation of Al₂O₃-EG/W nanofluid flow inside parabolic trough solar collector. *Renew Energy* 129:473–485. <https://doi.org/10.1016/j.renene.2018.06.023>
44. Ebrahimi-Moghadam A, Farzaneh-Gord M (2022) Optimal operation of a multi-generation district energy hub based on electrical, heating, and cooling demands and hydrogen production. *Appl Energy* 309:118453. <https://doi.org/10.1016/j.apenergy.2021.118453>
45. Wang A, Wang S, Ebrahimi-Moghadam A et al (2022) Techno-economic and techno-environmental assessment and multi-objective optimization of a new CCHP system based on waste heat recovery from regenerative Brayton cycle. *Energy* 241:122521. <https://doi.org/10.1016/j.energy.2021.122521>
46. Tavakoli A, Farzaneh-Gord M, Ebrahimi-Moghadam A (2023) Using internal sinusoidal fins and phase change material for performance enhancement of thermal energy storage systems: Heat transfer and entropy generation analyses. *Renew Energy* 205:222–237. <https://doi.org/10.1016/j.renene.2023.01.074>
47. Ebrahimi-Moghadam A, Kowsari S, Farhadi F, Deymi-Dashtebayaz M (2020) Thermohydraulic sensitivity analysis and multi-objective optimization of Fe₃O₄/H₂O nanofluid flow inside U-bend heat exchangers with helical coil inserts. *Appl Therm Eng* 164:114518. <https://doi.org/10.1016/j.applthermaleng.2019.114518>
48. Ebrahimi-Moghadam A, Gohari F, Hoseinzade D, Deymi-Dashtebayaz M (2020) A comprehensive thermo-hydraulic analysis and optimization of turbulent TiO₂/W-EG nano-fluid flow inside double-pipe heat exchangers with helical coil inserts. *J Brazilian Soc Mech Sci Eng* 42:232. <https://doi.org/10.1007/s40430-020-02320-7>
49. Mohseni-Gharyehsafa B, Ebrahimi-Moghadam A, Okati V et al (2019) Optimizing flow properties of the different nanofluids inside a circular tube by using entropy generation minimization approach. *J Therm Anal Calorim* 135:801–811. <https://doi.org/10.1007/s10973-018-7276-x>
50. Nilpueng K, Asirvatham LG, Dalkılıç AS et al (2020) Heat transfer and fluid flow characteristics in a plate heat exchanger filled with copper foam. *Heat Mass Transf* 56:3261–3271
51. Arasteh H, Rahbari A, Mashayekhi R et al (2021) Effect of pitch distance of rotational twisted tape on the heat transfer and fluid flow characteristics. *Int J Therm Sci* 170:106966
52. Lin H, Wu X, Ayed H et al (2022) A new biomass gasification driven hybrid system for power and liquid hydrogen cogeneration: Parametric study and multi-objective evolutionary optimization. *Int J Hydrogen Energy* 47:26394–26407. <https://doi.org/10.1016/j.ijhydene.2022.01.110>
53. Ebrahimi-Moghadam A, Farzaneh-Gord M, Jabari Moghadam A et al (2021) Design and multi-criteria optimisation of a trigeneration district energy system based on gas turbine, Kalina, and ejector cycles: Exergoeconomic and exergoenvironmental evaluation. *Energy Convers Manag* 227:113581. <https://doi.org/10.1016/j.enconman.2020.113581>
54. Li Z, Wang J, Huang J, Ding M (2023) Development and research of triangle-filter convolution neural network for fuel reloading optimization of block-type HTGRs. *Appl Soft Comput* 136:110126. <https://doi.org/10.1016/j.asoc.2023.110126>
55. Yan A, Xiang J, Cao A et al (2022) Quadruple and Sextuple Cross-Coupled SRAM Cell Designs With Optimized Overhead for Reliable Applications. *IEEE Trans Device Mater Reliab* 22:282–295. <https://doi.org/10.1109/TDMR.2022.3175324>
56. Li B, Tan Y, Wu A-G, Duan G-R (2022) A Distributionally Robust Optimization Based Method for Stochastic Model Predictive Control. *IEEE Trans Automat Contr* 67:5762–5776. <https://doi.org/10.1109/TAC.2021.3124750>

57. Alirahmi SM, Ebrahimi-Moghadam A (2022) Comparative study, working fluid selection, and optimal design of three systems for electricity and freshwater based on solid oxide fuel cell mover cycle. *Appl Energy* 323:119545. <https://doi.org/10.1016/j.apenergy.2022.119545>
58. Ebrahimi-Moghadam A, Farzaneh-Gord M (2021) Energy, exergy, and eco-environment modeling of proton exchange membrane electrolyzer coupled with power cycles: Application in natural gas pressure reduction stations. *J Power Sources* 512:230490. <https://doi.org/10.1016/j.jpowsour.2021.230490>
59. Islam MS, Saha SC (2021) Heat transfer enhancement of modified flat plate heat exchanger. *Appl Therm Eng* 186:116533

Publisher's Note Springer Nature remains neutral with regard to jurisdictional claims in published maps and institutional affiliations.

Springer Nature or its licensor (e.g. a society or other partner) holds exclusive rights to this article under a publishing agreement with the author(s) or other rightsholder(s); author self-archiving of the accepted manuscript version of this article is solely governed by the terms of such publishing agreement and applicable law.